Experimental Details

Materials. All syntheses and manipulations were conducted in an N_2-filled drybox (Vacuum Atmospheres, $O_2 < 0.2$ ppm, $H_2O < 0.5$ ppm) or using standard Schlenk techniques under an atmosphere of Ar unless otherwise noted. Tetrahydrofuran (THF) and 2-methyltetrahydrofuran (2-MeTHF) inhibitor-free were purchased from Sigma-Aldrich and distilled under argon from sodium/benzophenone. All solvents were degassed by a minimum of three freeze-pump-thaw cycles and stored over freshly activated 3 Å molecular sieves in the drybox following distillation. The ligand 5, 10, 15-tris((2,4,6-triphenyl)phenyl)corrole ($ttppcH_3$), as well as the metalated Fe^{III}(ttppc), were synthesized according to a published procedures.[1] The isotopically pure $^{18}O_2$ (98 atom %) was purchased from ICON Isotopes (Summit, NJ). The compounds TEMPOH, TEMPOD and 2,6-di-tert-butyl-4-methoxyphenol were synthesized according to published procedures.[2-4] All other reagents were purchased from commercial vendors and used without further purification.

Instrumentation. The ^{1}H NMR spectra were measured on a Bruker 300 MHz or a Bruker 400 MHz spectrometer. Solution magnetic susceptibilities were determined by a simplified Evans method.[5] UV−vis experiments were carried out on a Cary bio-50 or Cary 60 UV−vis spectrophotometer equipped with a Unisoku USP-203A cryostat using a 1 cm modified Schlenk cuvette. EPR measurements were performed on a Bruker X-band EPR spectrometer in 4 mm quartz EPR tubes (Wilmad).

Preparation of sodium/mercury amalgam. In an N_2-filled glovebox, freshly cut Na metal (~10 mg) was added to Hg (700 mg) to form a Na/Hg (1.5%) amalgam. This amount of Na/Hg can be used to reduce multiple samples of Fe^{III}(ttppc) solutions of varying concentrations.

Synthesis of $[Fe^{II}(ttppc)]^-$ (1). To a solution of Fe^{III}(ttppc) in either THF or MeTHF was added a 1.5% Na/Hg amalgam (700 mg). Stirring was carried out with a glass-covered magnetic stir-bar to agitate the surface of the amalgam and facilitate the reduction. The reaction was stirred for 10-15 min at lower concentrations (~20 – 25 μM, 2 mL e.g. for UV-vis) of the iron complex and 3-5 min for higher concentrations (~2.5 mM, 500 μL e.g. for NMR, EPR, rRaman and Mössbauer), to ensure complete reduction. Complete reduction was indicated by a color change from red-brown (Fe^{III}(ttppc)) to green ($[Fe^{II}(ttppc)]^-$), and was verified by UV–vis spectroscopy.

Preparation of Mossbauer samples for 1 and 2. For **1**, a solution of ^{57}Fe-enriched (95.5% isotopic purity) Fe^{III}(ttppc) in THF (4 mM) was reduced to $[Fe^{II}(ttppc)]^-$ in situ at 25 °C. This solution was transferred to a Delrin Mössbauer cup, which was placed in a sealed vial. The sample was frozen and stored at 77 K until loaded into the Mössbauer spectrometer

For Mössbauer samples for **2,** a solution of **1** was similarly prepared in a Mössbauer cup and sealed in a vial, as noted above. The vial containing **1** was then immersed in a cold bath of acetone/liquid N_2 at -80 °C to thermally equilibrate. An amount of O_2 gas (2.5 mL) was measured via gas-tight syringe and then bubbled through the solution, resulting in the formation of a green-brown solution. After the introduction of O_2, the vial was then immersed and stored in liquid N_2 until loaded into the Mössbauer spectrometer.

Evans Method measurement. A 500 μL solution of **1** (3.0 mM) in THF-d_8 containing toluene (25 μL) as a reference was placed in an NMR tube with a coaxial inner tube containing blank solvent with the same toluene reference. A ^{1}H NMR spectrum was recorded at 298 K and the chemical shift of the toluene peak in the presence of the paramagnetic **1** was compared to that of the toluene peak in the inner tube containing only solvent. The effective spin-only magnetic moment was calculated from the following equation:

$$\mu_{eff} = 0.0618\sqrt{\frac{\Delta\nu T}{2fM}}$$

where:

f = oscillator frequency (MHz) of spectrometer

$\Delta\nu$ = difference in frequency (Hz) between reference signals

T = temperature in K

M = molar concentration of compound

Spectral titration. An O_2-saturated solution of THF was prepared by sparging dry THF with dry O_2 for 20 min at 25 °C (10 mM).[6-7] This stock solution was diluted to give a 1.0 mM solution of O_2, which was then added by gas-tight syringe to a solution of **1** in THF (2.5 mL, 24 μM) at -80 °C. The O_2 solution was added in sequential aliquots of 20 μL (0.3 equiv). The formation of **2** was monitored by following an increase in absorbance at 454 nm. Full formation of **2** was reached with 1.2 equiv of O_2 consistent with a 1:1 Fe:O_2 binding stoichiometry.

Preparation of Resonance Raman samples. A stock solution of **1** was prepared in 2-MeTHF or THF (2.7 mM). An aliquot of the stock solution of **1** was transferred to a 5 mm NMR tube and sealed in a drybox. The NMR tube was removed from the drybox and cooled to the desired temperature. Using a three-way gastight syringe, 2 mL of $^{16}O_2$ (natural abundance) or $^{18}O_2$ (98%) was added to the solution of **1**, yielding a color change from green to brown-green. The reaction was allowed to proceed with frequent manual mixing for 5 min, and then the reaction mixture was slowly annealed in liquid nitrogen and stored at 77 K until needed. Resonance Raman spectra were obtained on samples maintained at 110 K during data acquisition using a cold-finger holder in a glass Dewar filled with liquid nitrogen. The 458-nm line of an Ar laser (Innova 90, Coherent) was used with a backscattering geometry and a cylindrical lens that focuses the laser beam along the axis of the NMR tube. The backscattered photons were collected with a camera lens and focused on the entrance slit of a McPherson 2061/207 spectrograph equipped with a liquid-nitrogen-cooled CCD camera (LN-1100PB, Princeton Instruments). A long-pass filter (RazorEdge, Semrock) was used to attenuate the Rayleigh scattering. Rapid acquisition measurements with a range of laser power and rapid continuous sample spinning revealed a lack of photosensitivity of the samples as long as the laser power was maintained ≤ 20 mW. Frequencies were calibrated using aspirin and are accurate to ±1 cm^{-1}.

Preparation of EPR samples for quantitation of TEMPO Radical. A 250 μL solution of **1** was prepared in 2-MeTHF (2.0 mM) and an amount of TEMPOH (50 μL, 3 equiv) was added. The mixture was transferred to a 4 mm EPR tube and cooled to −40 °C. An excess of O_2(g) (~2.5 mL)

was added, resulting in the formation of a green-brown solution. The reaction was allowed to proceed for 1 h, and then the tube was slowly annealed and stored at 77 K until an EPR spectrum could be recorded. Quantification of the TEMPO radical product was determined by double integration and comparison against a calibration curve of an external TEMPO radical standard.

Quantitation of indole dioxygenation product. A solution of **1** in THF-d_8 was transferred to a 5 mm NMR tube and cooled to −40 °C. An amount of excess O_2 gas (~2.5 mL) was added, resulting in the formation of a green-brown solution. An amount of 2,3-dimethylindole was added and the reaction was allowed to proceed to completion then warmed up to room temperature. The internal standard trimethoxybenzene was added and yields were calculated based on selected integrated peaks using the formula below where *n* represents the number of moles and *I* represents the peak integration.

$$\% \text{ yield} = \frac{n_{std} \times \frac{I_{pdt}}{I_{std}} \times \frac{3}{1}}{n_{Fe\ complex}}$$

Control reactions of 1) **1** + 2,3-dimethylindole, 2) 2,3-dimethylindole + O_2 and 3) 2,3-dimethylindole + KO_2/kryptofix were run under similar conditions. No significant amounts of product were detected in these reactions.

Kinetic Studies. *a) TEMPOH:* A solution of **1** in THF (19 μM, 3.0 mL) was generated in situ. Varying amounts of substrate equivalents resulting in different effective concentrations (50 μL additions, ~30 – 150 equiv, 0.6 mM – 3.0 mM) were preloaded into the solution and cooled to desired temperature. Initial UV-Vis spectra of the solution shows spectrum expected for **1** even after prolonged time period, confirming that there is no reactivity between starting material **1** and substrates. Upon bubbling of 500 μL of O_2 gas (measured by gas tight syringe) into the solution, full formation of the **2** was observed followed by decay over time as monitored by UV-vis spectroscopy.

b) For 2,3-dimethylindole substrate: A solution of **1** in THF (60 μM, 2.0 mL) was generated in situ. Varying amounts of substrate equivalents resulting in different effective concentrations (50 μL additions, 70 – 300 equiv, 4 mM – 18 mM) were preloaded into the solution and cooled to the desired temperature. Initial UV-vis spectra of the solution shows the spectrum expected for **1** even after prolonged times, confirming that there is no reactivity between starting material **1** and substrate. Upon bubbling of 500 μL of O_2 gas (measured by gas tight syringe) into the solution, full formation of **2** was observed followed by decay over time as monitored by UV-vis spectroscopy.

For all reactions, the pseudo-first-order rate constants (k_{obs}) for these reactions were obtained by nonlinear least-squares fitting of the plots of absorbance at 595 nm (for 2,3-DMI) or 454 nm (for TEMPOH) (Abs_t) versus time (t) according to the equation $Abs_t = Abs_f + (Abs_0 - Abs_f) \exp(-k_{obs}t)$, where Abs_0 and Abs_f are initial and final absorbance, respectively. Second-order rate constants (k_2) were obtained from the slope of the best-fit line from a plot of k_{obs} versus substrate concentration.

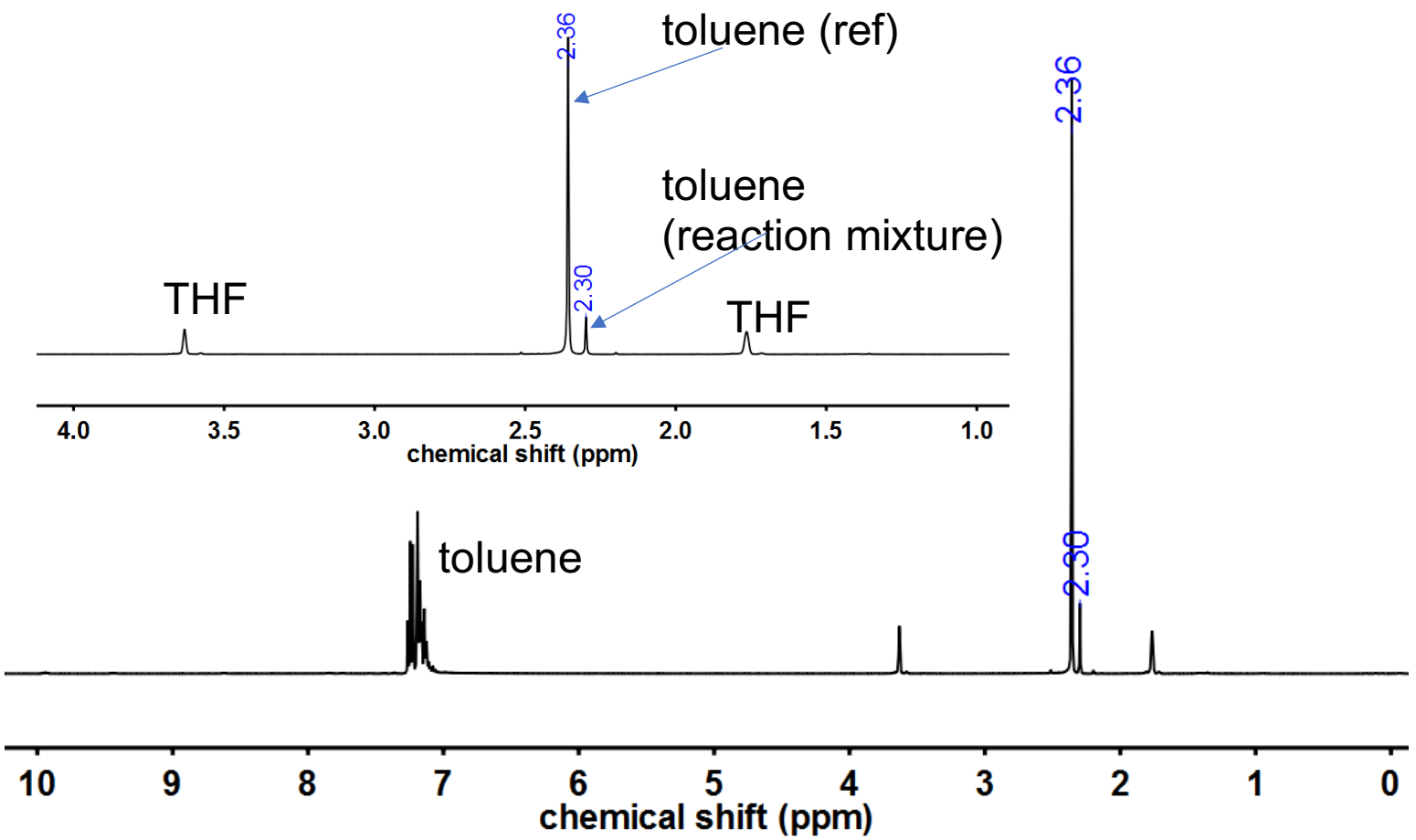

Figure S1. Evans method ^{1}H-NMR spectrum of **1** (3.0 mM) in THF-d_8 with toluene as reference.

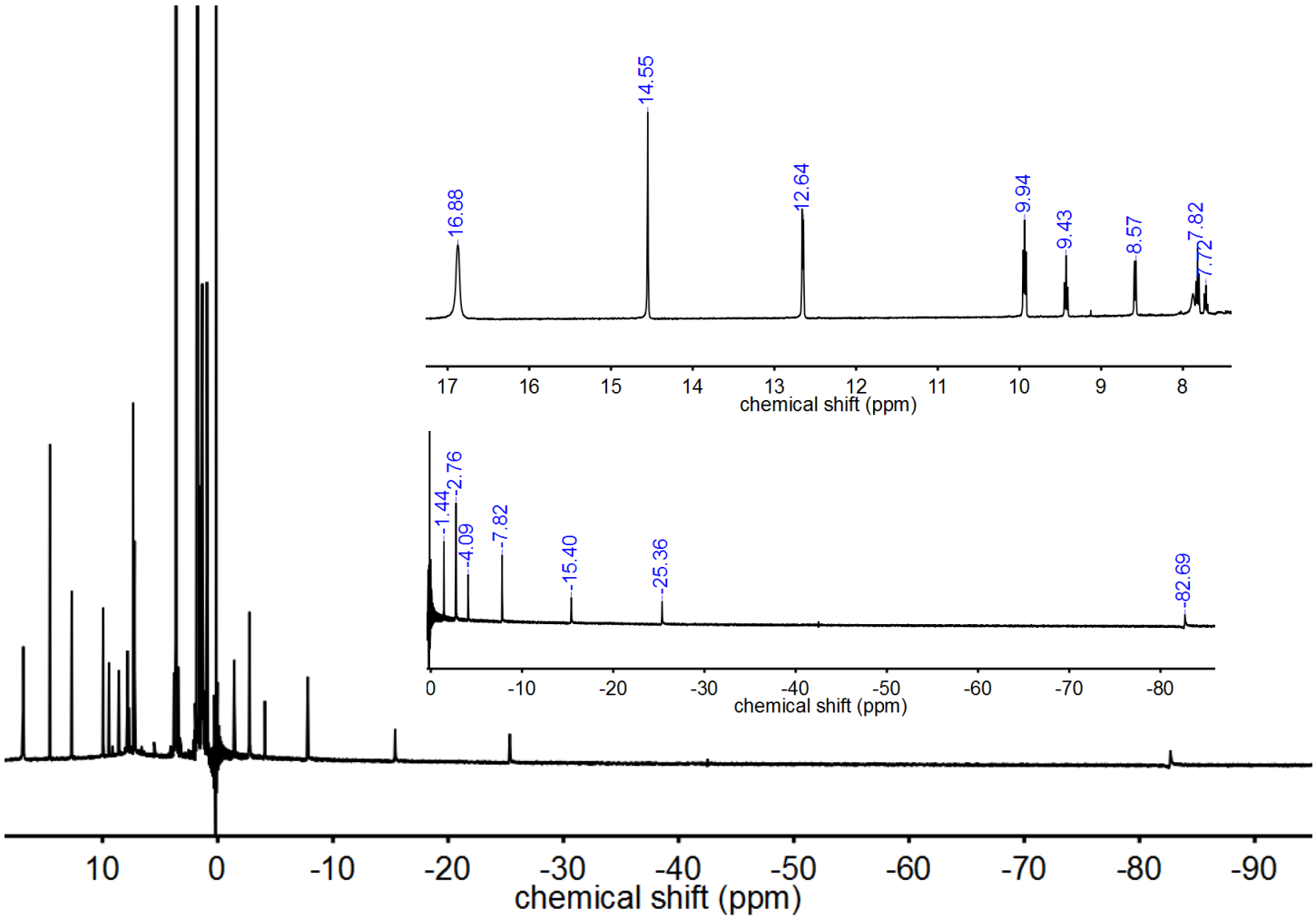

Figure S2. ^{1}H NMR spectrum (400 MHz) of [Fe^{II}(ttppc)]- (**1**) in THF-d_8 at 25 °C. Inset: Expanded region from 8 to 17 ppm (top) and -85 to 0 ppm (bottom). ^{1}H NMR (400 MHz, THF-d_8) δ (ppm): 16.88 (s, br), 14.55 (s), 12.64 (d), 9.94 (t), 9.43 (t), 8.57 (d), 7.82 (t), 7.72 (t), -1.44 (s), -2.76 (s), -4.09 (s), -7.82 (s), -15.40 (s), -25.36 (s), -82.69 (s, br).

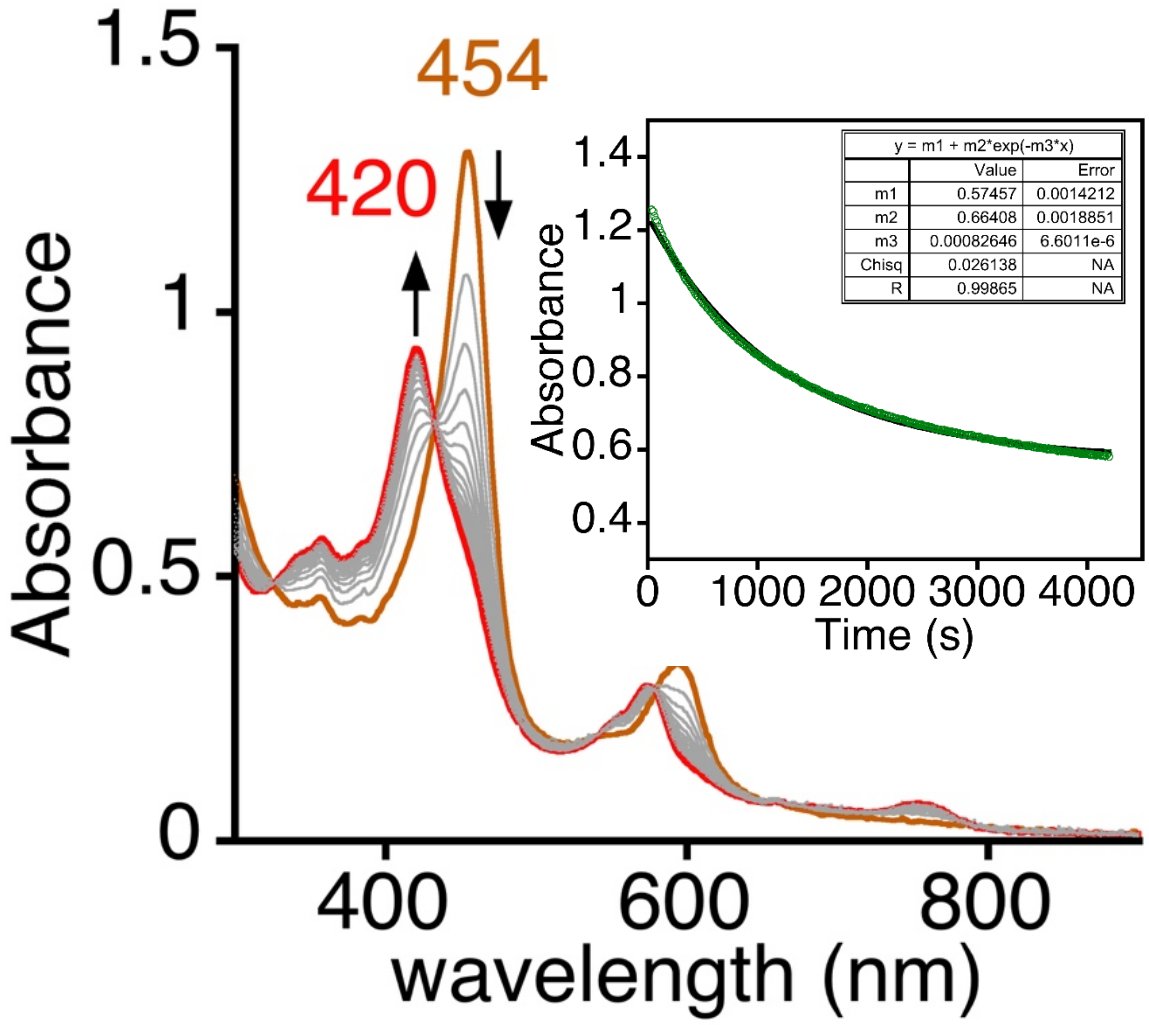

Figure S3. Time-resolved UV-vis spectral changes (0 – 90 min) observed for the self-decay of **2** (19 μM) to form Fe^{III}(ttppc) in THF at -40 °C. Inset: changes in absorbances at 454 nm over time with best-fit line (black) for first-order decay with k_{decay} = 0.000826 s^{-1}.

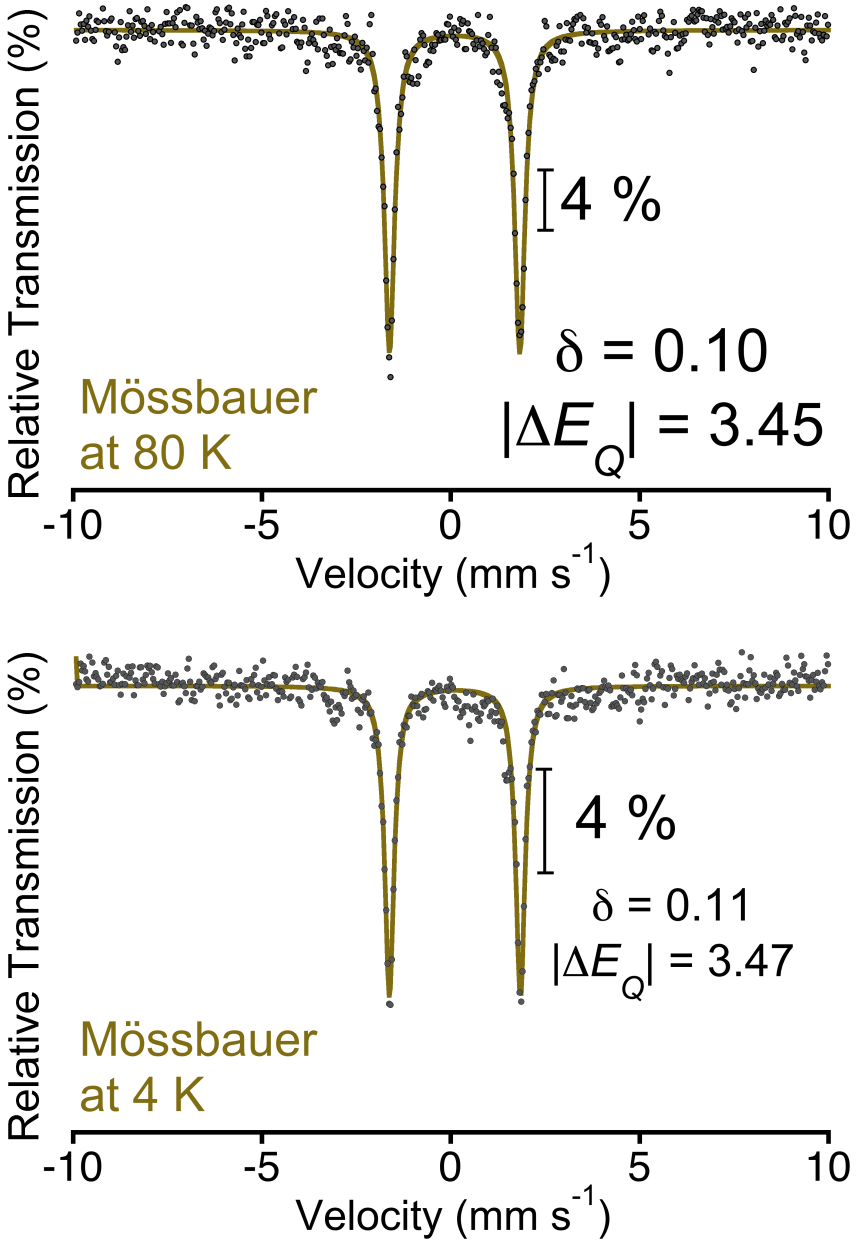

Figure S4 Mössbauer spectra of **2** in 2-MeTHF at 80 K (top): $\delta = 0.10$ mm/s, $\Delta E_Q = 3.45$ mm/s, **2** in 2-MeTHF at 4 K (bottom): $\delta = 0.11$ mm/s, $\Delta E_Q = 3.47$ mm/s.

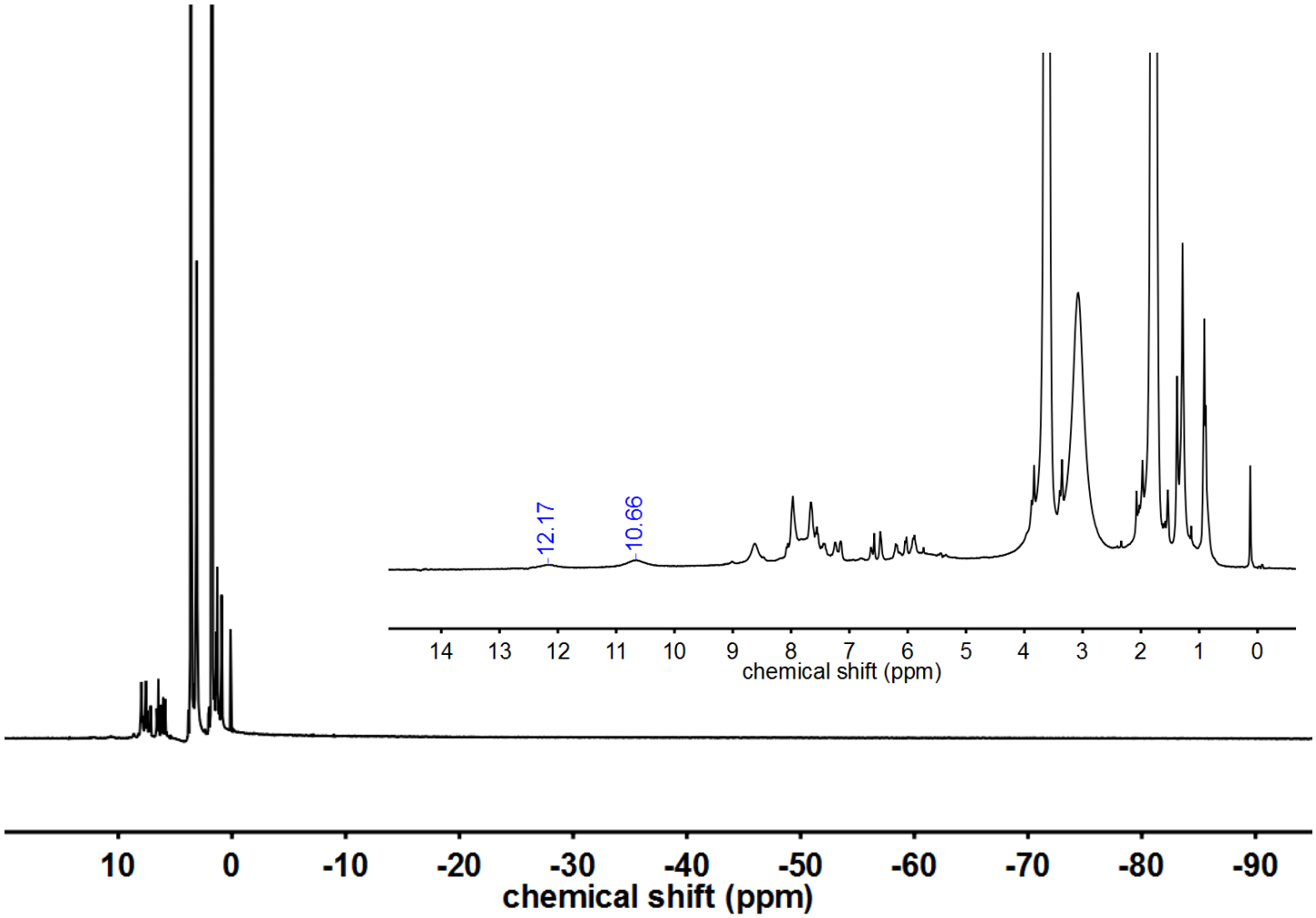

Figure S5. ^{1}H NMR (400 MHz) of $[Fe^{III}(ttppc)(O_2)]^-$ (**2**) in THF-d_8 at -80 °C. Inset: Expanded region from 0 – 15 ppm showing minor Fe^{III}(ttppc) decay product indicated by the broad peaks at 12.17 (s, br) and 10.66 (s, br).

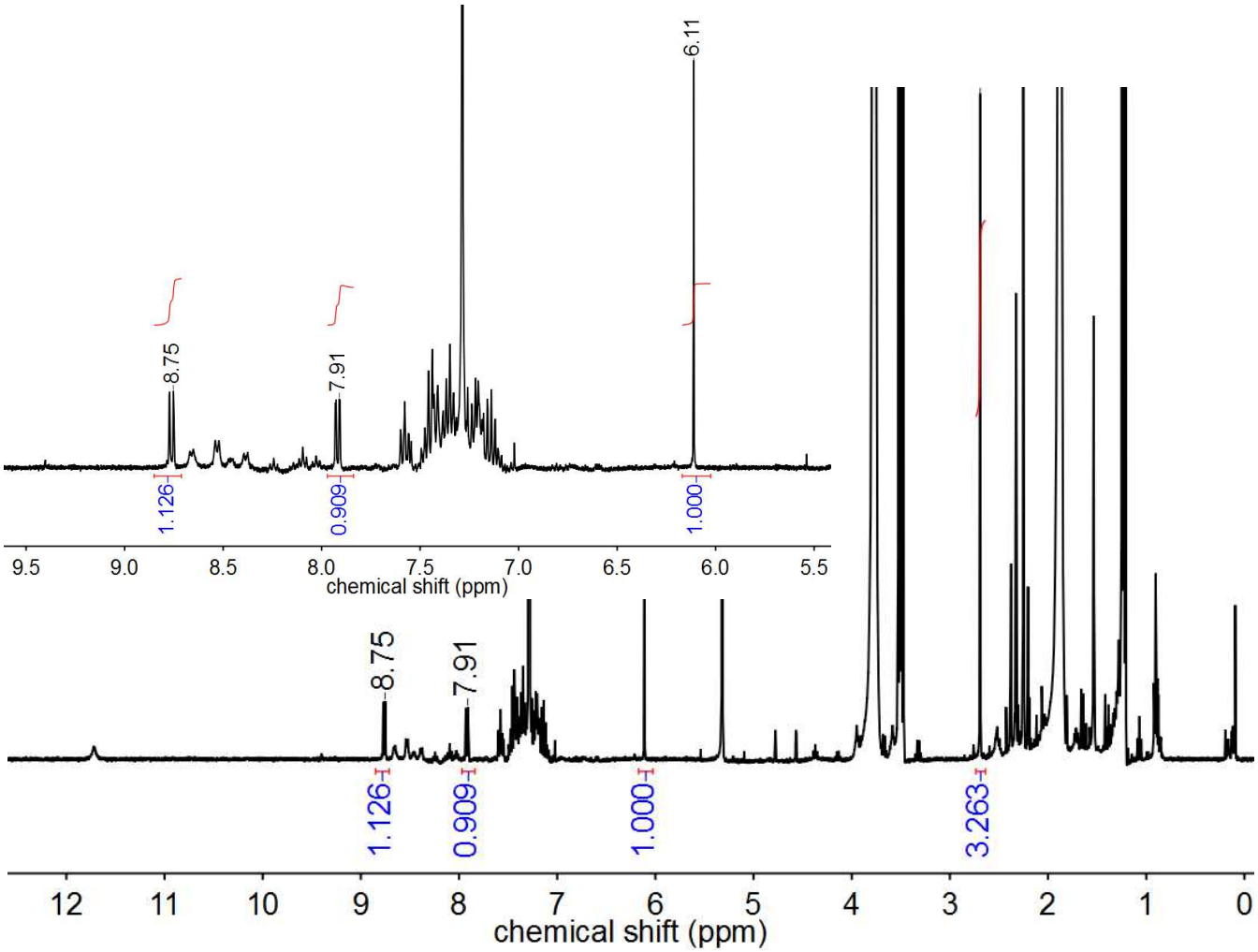

Figure S6. ^{1}H NMR spectra for the reaction of **2** (2.2 µmol, 3.1 mM in 700 µL) with 2,3-DMI (10 µmol, 5 equiv). The reaction was run at -40 °C, visually monitored for completion (solution color change from brown-green to red), and then warmed to 23 °C. The internal standard 1,3,5-trimethoxybenzene (0.62 µmol) was added prior to data collection. The peaks corresponding to the phenyl protons of *N*-(2-acetyl-phenyl)-acetamide, at 8.75 ppm (d, 1H) and 7.91 ppm (d, 1H), were integrated and compared to the standard at 6.11 ppm (s, 3H). Average yield for *N*-(2-acetyl-phenyl)-acetamide was 86 ± 7% (2 trials).

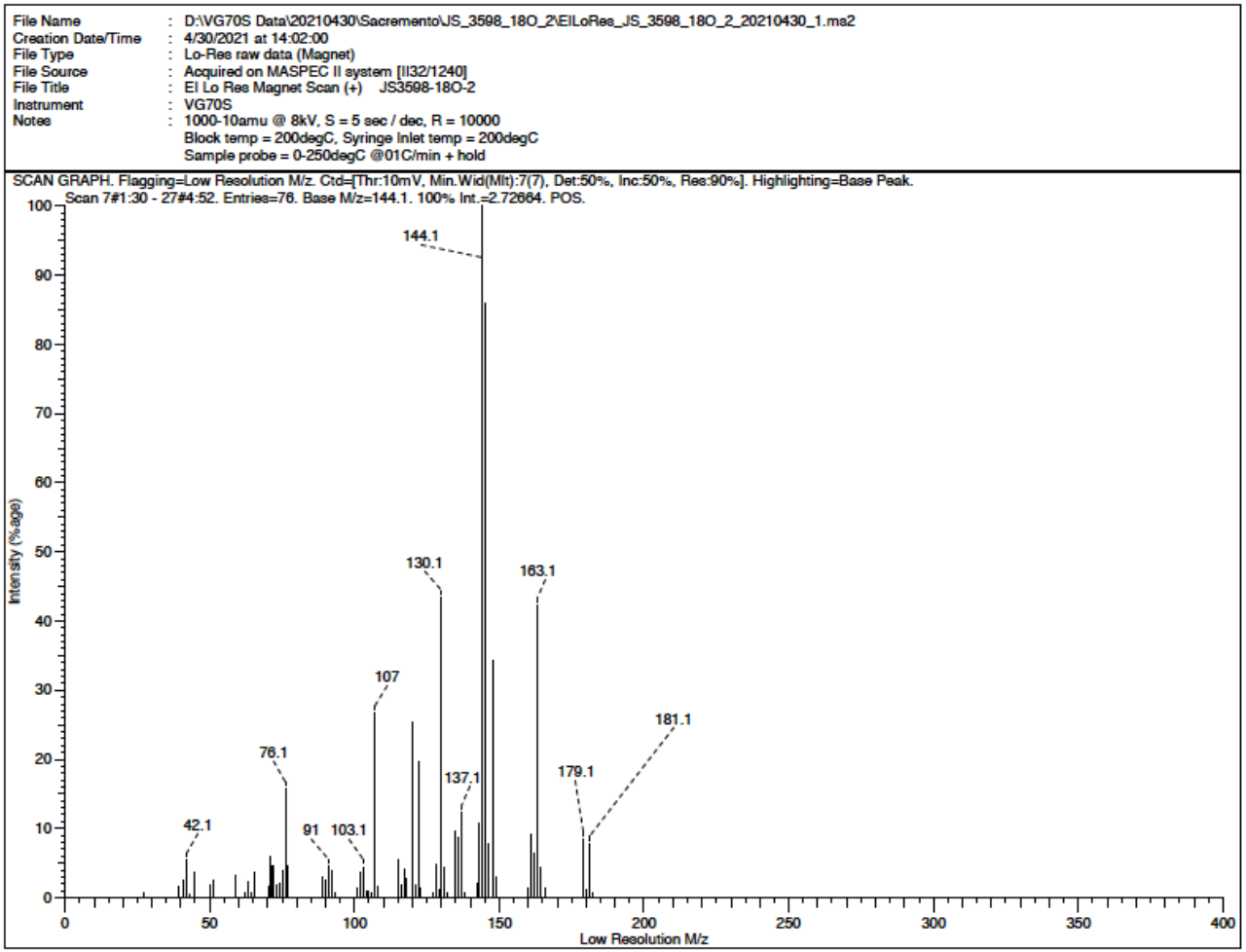

Figure S7. EI-MS data for the organic product from **1** + 2,3-DMI + $^{18}O_2$ in THF at -40 C°. The peak at 181.1 *m/z* is assigned to the ^{18}O-labeled *N*-(2-acetyl-phenyl)-acetamide, $C_{10}H_{11}N^{18}O_2$: Calcd 181.20 *m/z*.

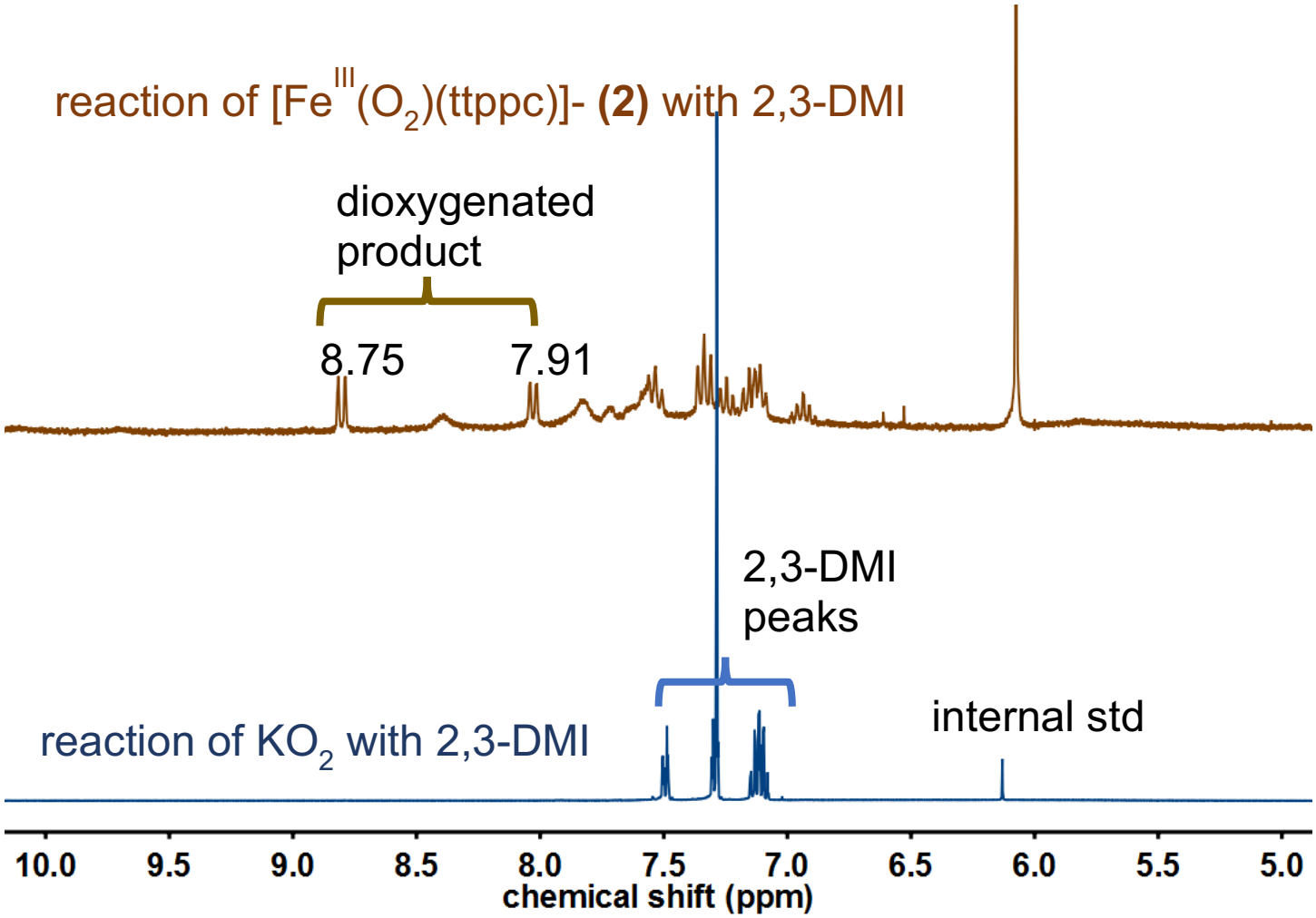

Figure S8. ^{1}H-NMR spectrum of KO_2/kryptofix (1:1) (3 mM) + 2,3-DMI (5 equiv) in THF-d^8. The mixture was incubated for 2 h at -40 °C, and then warmed to 23 °C followed by acquisition of the spectrum. Reaction of **2** (3.1 mM) with 2,3-DMI (5 equiv) is shown for comparison.

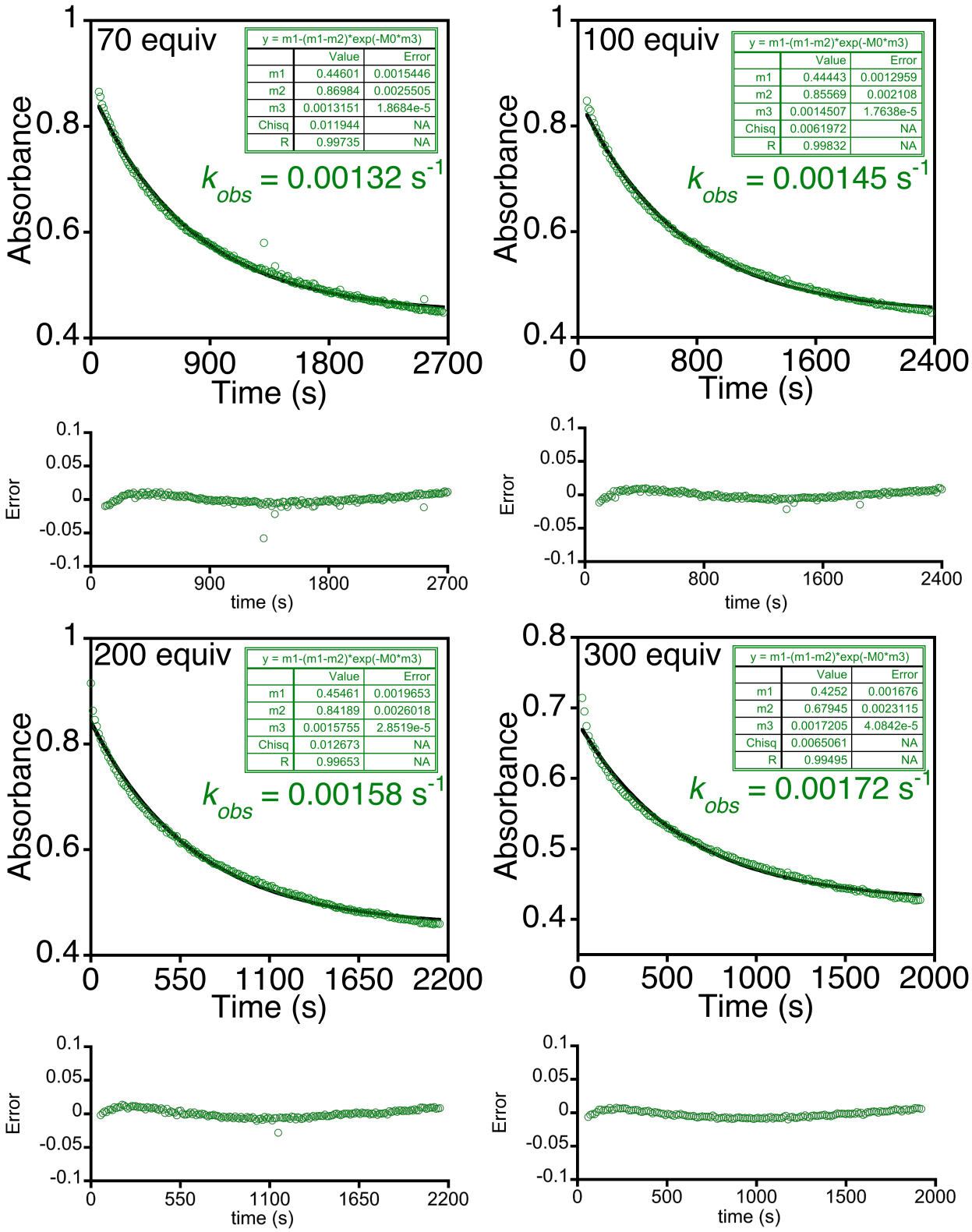

Figure S9. Plots of the change in absorbance versus time for the decay of **2** (595 nm) (green) with the best fit lines for the reaction of **2** (60 μM) with 2,3-DMI (a-d: 70, 100, 200, 300 equiv) in THF at -40 °C. Residuals plotted as absolute error from expression.

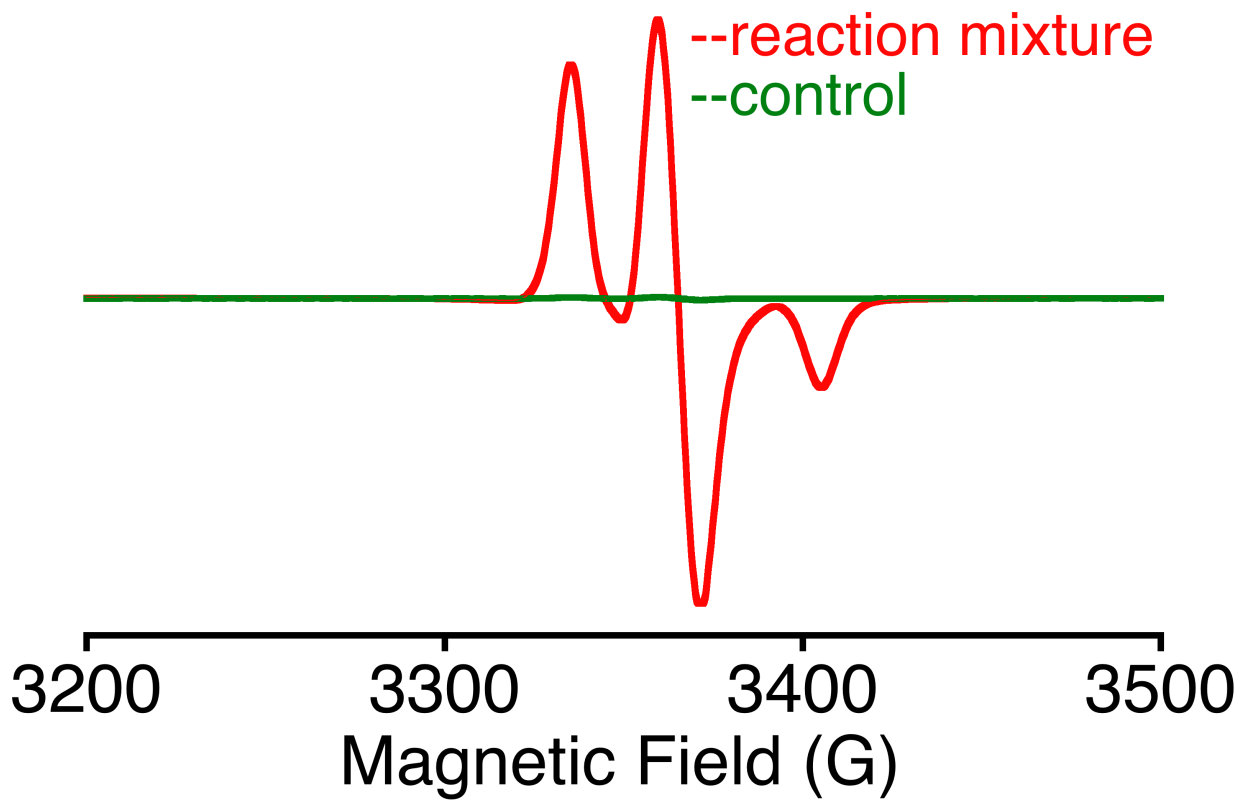

Figure S10. EPR spectrum (9.77 GHz) at 12 K for the reaction of **2** with TEMPOH (red line) in 2-MeTHF showing the expected signal for TEMPO• centered at *g* 2.00.[8] Double integration and comparison with a calibration curve gives a 97% yield of TEMPO• (average of 2 runs). In comparison, the TEMPOH in 2-MeTHF in the absence of **2** (green line) exhibits a TEMPO• signal of ~3%. Experimental conditions: Microwave power = 0.2 mW; Modulation amplitude = 1 G, Receiver gain = 5 x 10^3.

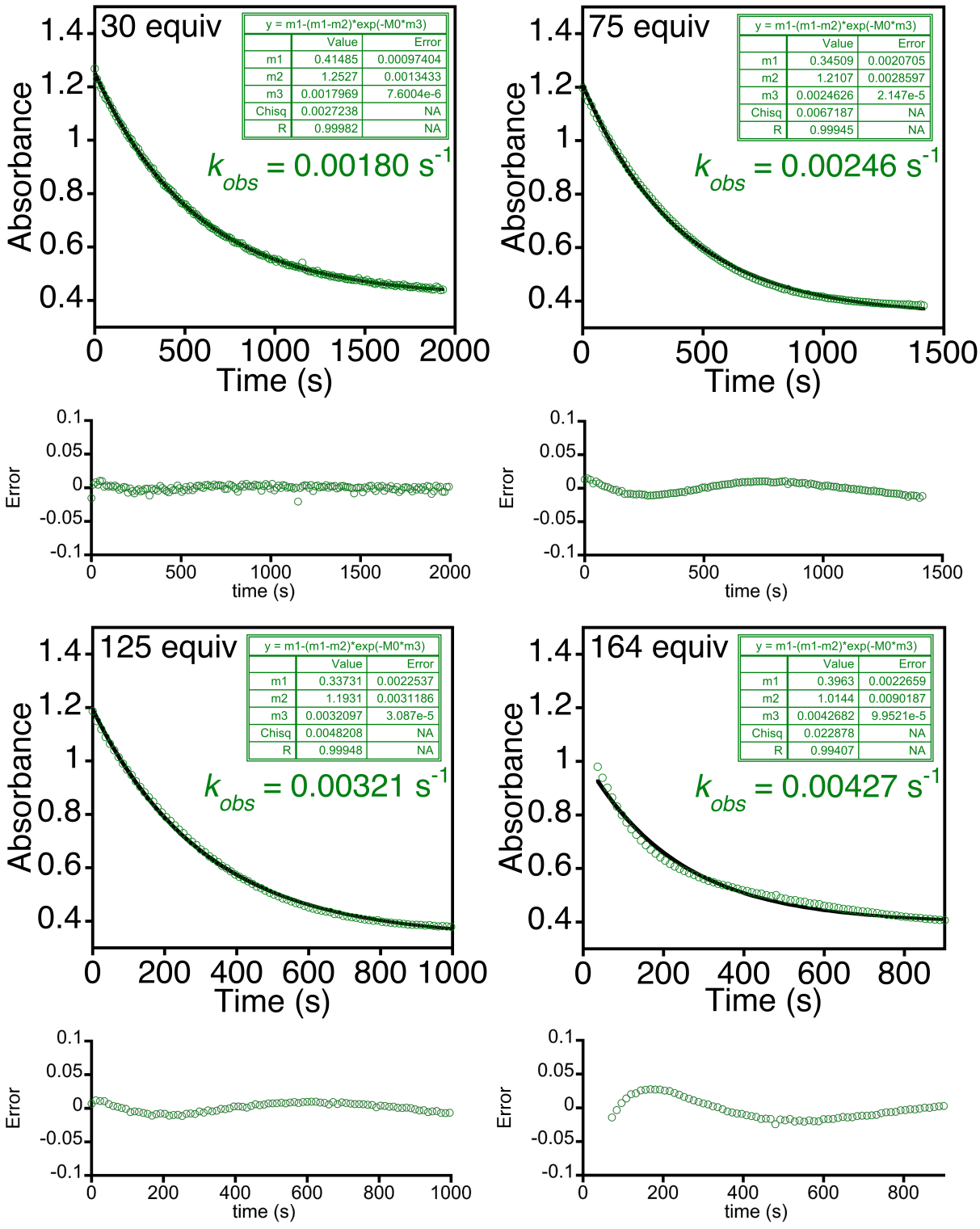

Figure S11. Plots of the change in absorbance versus time for the decay of **2** (454 nm) (green) with the best fit lines for the reaction of **2** (19 μM) with TEMPOH (30, 75, 125, 164 equiv) in THF at -40 °C.

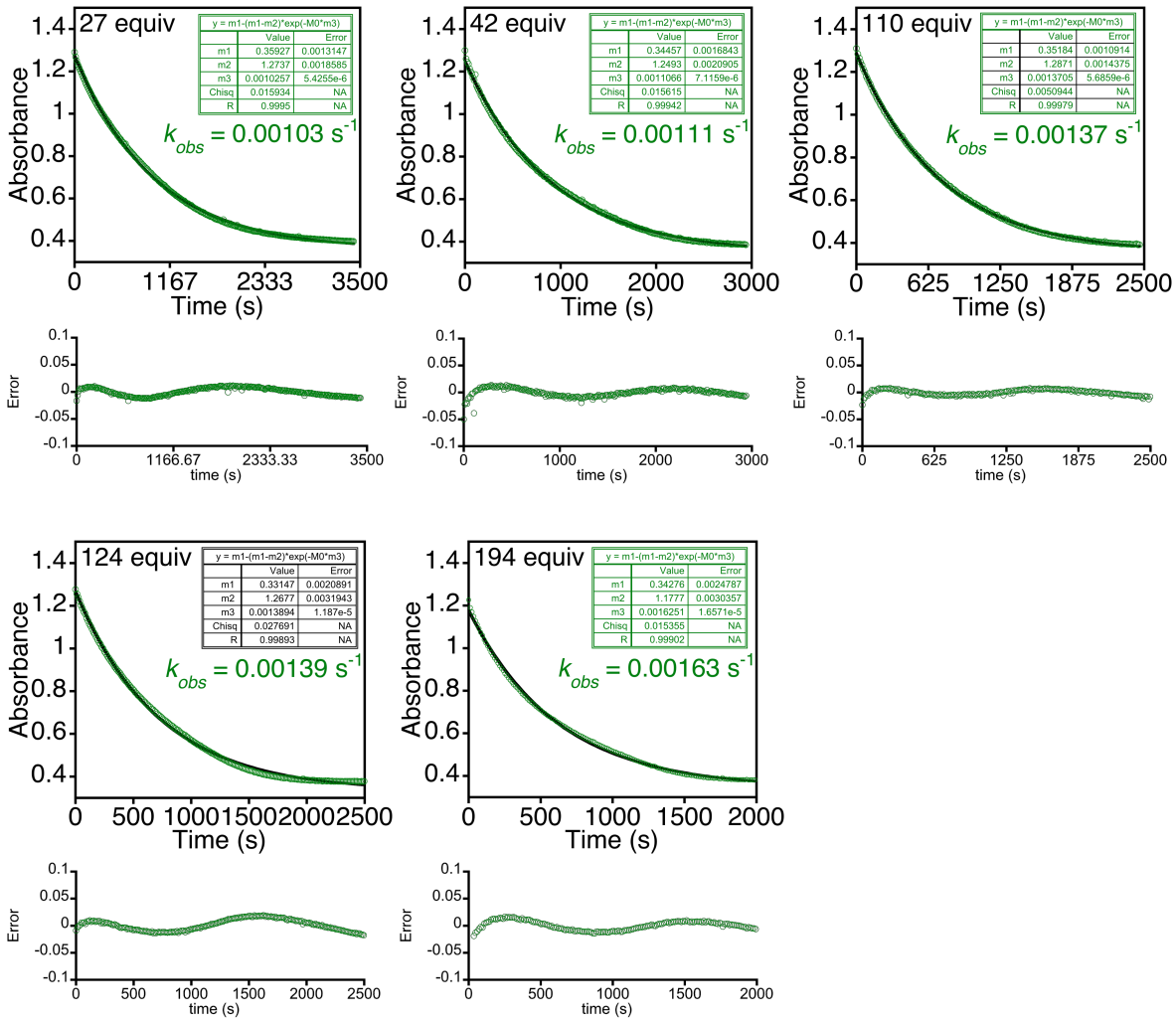

Figure S12. Plots of the change in absorbance versus time for the decay of **2** (454 nm) (green) with the best fit lines for the reaction of **2** (19 μM) with TEMPOD (27, 42, 110, 124, 194 equiv) in THF at -40 °C.

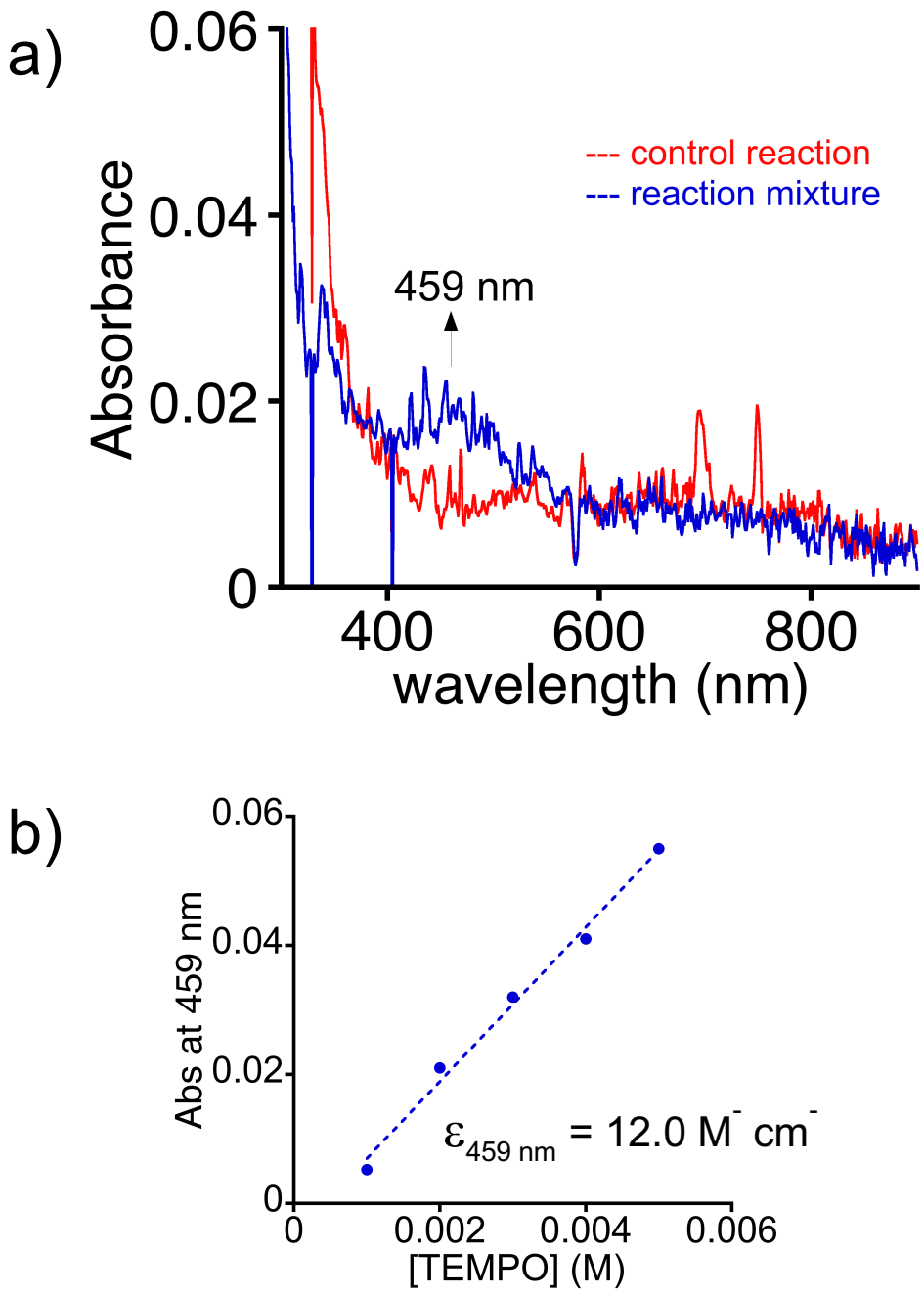

Figure S13. a) UV-vis spectra of the reaction of KO_2 (2.8 mM) and kryptofix (3.6 mM) with TEMPOH (5 equiv) (blue), and TEMPOH alone (0.015 M) (red) in THF/MeCN (4:1) at -40 °C. Absorbance at 459 nm indicates formation of TEMPO•. Although the noise in the spectra make quantitation challenging, the absorbance for TEMPO• gives ~66% yield of TEMPO• with respect to the starting $O_2^{-\bullet}$ concentration based on a calibration curve constructed from solutions of TEMPO• in varying concentration (0.001 – 0.005 M) in a KO_2 solution (3.1 mM). Higher

concentrations were not used because this control reaction was designed to mimic the conditions employed in the reaction of **2** with TEMPOH.

Single X-ray Crystal Crystallography

All reflection intensities were measured at 110(2) K using a SuperNova diffractometer (equipped with Atlas detector) with Cu *K*α radiation (λ = 1.54178 Å) under the program CrysAlisPro (Version CrysAlisPro 1.171.39.29c, Rigaku OD, 2017). The same program was used to refine the cell dimensions and for data reduction. The structure was solved with the program SHELXS-2018/3 (Sheldrick, 2018) and was refined on F^2 with SHELXL-2018/3 (Sheldrick, 2018). Analytical numeric absorption correction using a multifaceted crystal model was applied using CrysAlisPro. The temperature of the data collection was controlled using the system Cryojet (manufactured by Oxford Instruments). The H atoms were placed at calculated positions using the instructions AFIX 13, AFIX 23, AFIX 43 or AFIX 137 with isotropic displacement parameters having values 1.2 or 1.5 U_{eq} of the attached C atoms.

One of the phenyl groups and the three methyl THF solvent molecules are disordered over two orientations, and the occupancy factors of the major / minor components of the disorder can be retrieved from the final .cif file.

Table S1. Single Crystal X-ray Crystallography Experimental Details

	xs2643a
Crystal data	
Chemical formula	$C_{96}H_{69}FeN_4NaO_2 \cdot 2(C_5H_{10}O)$
M_r	1561.65
Crystal system, space group	Triclinic, *P*-1
Temperature (K)	110
a, *b*, *c* (Å)	14.0413 (9), 16.2509 (8), 20.5767 (11)
α, β, γ (°)	96.602 (4), 107.820 (5), 109.798 (5)
V (Å^3)	4078.6 (4)
Z	2
Radiation type	Cu *K*α
μ (mm^{-1})	1.99
Crystal size (mm)	0.20 × 0.12 × 0.11
Data collection	
Diffractometer	SuperNova, Dual, Cu at zero, Atlas

Absorption correction	Analytical *CrysAlis PRO* 1.171.41.93a (Rigaku Oxford Diffraction, 2020) Analytical numeric absorption correction using a multifaceted crystal model based on expressions derived by R.C. Clark & J.S. Reid. (Clark, R. C. & Reid, J. S. (1995). Acta Cryst. A51, 887-897) Empirical absorption correction using spherical harmonics, implemented in SCALE3 ABSPACK scaling algorithm.
T_{min}, T_{max}	0.747, 0.847
No. of measured, independent and observed [$I > 2\sigma(I)$] reflections	40556, 13363, 8811
R_{int}	0.084
$(\sin \theta/\lambda)_{max}$ (Å^{-1})	0.581
Refinement	
$R[F^2 > 2\sigma(F^2)]$, $wR(F^2)$, S	0.089, 0.271, 1.04
No. of reflections	13363
No. of parameters	1262
No. of restraints	916
H-atom treatment	H-atom parameters constrained
$\Delta\rho_{max}$, $\Delta\rho_{min}$ (e Å^{-3})	0.71, -0.53

Computer programs: *CrysAlis PRO* 1.171.39.29c (Rigaku OD, 2017), *SHELXS2018*/3 (Sheldrick, 2018), *SHELXL2018*/3 (Sheldrick, 2018), *SHELXTL* v6.10 (Sheldrick, 2008).

Table S2. Selected Bond Distances (Å) for [Na(H_2O)(2-MeTHF)(**1**)]

	Bond Distance (Å)
Fe1–N1	1.878(4)
Fe1–N2	1.879(4)
Fe1–N3	1.893(4)
Fe1–N4	1.862(4)
Fe–(23-atom)$_{plane}$	0.0440
N1–Na1	2.553(5)
O1–Na1	2.283(8)
O2S–Na1	2.270(6)
Na1–C28	2.861(7)
C_β– C_β (ave)	1.367(8)
C_α– C_β (ave)	1.425(7)
C_α– C_α (C1–C19)	1.420(7)

C_α–$N_{pyrrole}$ (ave)	1.380(7)
C_α–C_{meso} (ave)	1.408(7)

Table S3. Selected Bond Angles for [Na(H_2O)(2-MeTHF)(**1**)]

	Bond Angles (°)
N4–Fe1–N1	81.94(18)
N4–Fe1–N3	91.21(18)
N2–Fe1–N3	95.43(17)
N2–Fe1–N1	91.37(17)
N1–Na1–O1	117.1(3)
O2S–Na1–centroid (C26-C31)	93.6(4)
O2S–Na1–O1	106.5(2)
N1–Na1–centroid (C26-C31)	107.2(2)

REFERENCES:

1. Zaragoza, J. P. T.; Yosca, T. H.; Siegler, M. A.; Moenne-Loccoz, P.; Green, M. T.; Goldberg, D. P., Direct Observation of Oxygen Rebound with an Iron-Hydroxide Complex. *J. Am. Chem. Soc.* **2017,** *139*, 13640-13643.
2. Mader, E. A.; Davidson, E. R.; Mayer, J. M., Large Ground-State Entropy Changes for Hydrogen Atom
Transfer Reactions of Iron Complexes. *J. Am. Chem. Soc.* **2006,** *129*, 5153-5166.
3. Wu, A.; Mader, E. A.; Datta, A.; Hrovat, D. A.; Borden, W. T.; Mayer, J. M., Nitroxyl Radical Plus Hydroxylamine Pseudo Self-Exchange Reactions: Tunneling in Hydrogen Atom Transfer. *J. Am. Chem. Soc.* **2009,** *131*, 11985–11997.
4. Lee, J. Y.; Peterson, R. L.; Ohkubo, K.; Garcia-Bosch, I.; Himes, R. A.; Woertink, J.; Moore, C. D.; Solomon, E. I.; Fukuzumi, S.; Karlin, K. D., Mechanistic insights into the oxidation of substituted phenols via hydrogen atom abstraction by a cupric-superoxo complex. *J. Am. Chem. Soc.* **2014,** *136*, 9925-37.
5. Baglia, R. A.; Prokop-Prigge, K. A.; Neu, H. M.; Siegler, M. A.; Goldberg, D. P., Mn(V)(O) versus Cr(V)(O) Porphyrinoid Complexes: Structural Characterization and Implications for Basicity Controlling H-Atom Abstraction. *J. Am. Chem. Soc.* **2015,** *137*, 10874-10877.
6. Suenobu, T.; Arahori, I.; Nakayama, K. I.; Suzuki, T.; Katoh, R.; Nakagawa, T., Reaction of Oxygen with the Singlet Excited State of [n]Cycloparaphenylenes (n = 9, 12, and 15): A Time-Resolved Transient Absorption Study Seamlessly Covering Time Ranges from Subnanoseconds to Microseconds by the Randomly-Interleaved-Pulse-Train Method. *J. Phys. Chem. A* **2020,** *124*, 46-55.
7. Battino, R.; Rettich, T. R.; Tominaga, T., The Solubility of Oxygen and Ozone in Liquids. *J. Phys. Chem. Ref. Data* **1983,** *12*, 163-178.

8. Herb, K.; Tschaggelar, R.; Denninger, G.; Jeschke, G., Double resonance calibration of g factor standards: Carbon fibers as a high precision standard. *J. Magn. Reson.* **2018,** *289*, 100-106.